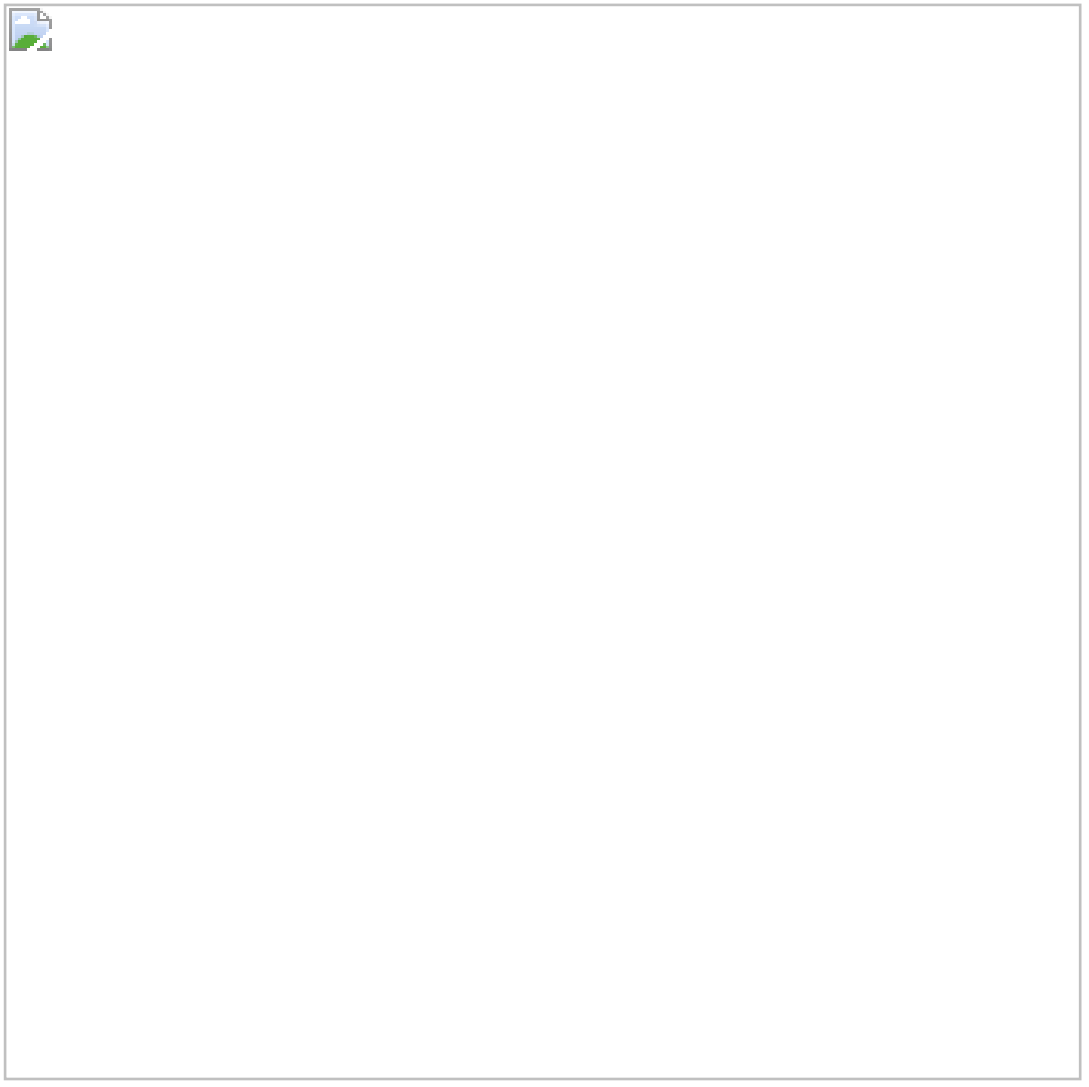

Modeling the Active-Layer Depth over the Tibetan Plateau

Authors: Oelke, Christoph, and Zhang, Tingjun

Source: Arctic, Antarctic, and Alpine Research, 39(4) : 714-722

Published By: Institute of Arctic and Alpine Research (INSTAAR), University of Colorado

URL: https://doi.org/10.1657/1523-0430(06-200)[OELKE]2.0.CO;2

Arctic, Antarctic, and Alpine Research, Vol. 39, No. 4, 2007, pp. 714–722

Modeling the Active-Layer Depth over the Tibetan Plateau

Christoph Oelke and Tingjun Zhang†*

*Institute for Geophysics, University of Münster, Corrensstr. 24, D-48149 Münster, Germany.
Corresponding author:
coelke@uni-muenster.de
†National Snow and Ice Data Center (NSIDC), Cooperative Institute for Research in Environmental Sciences (CIRES), University of Colorado, Boulder, CO 80309-0449, U.S.A.
tzhang@nsidc.org

Abstract

The soil thermal regime of the Tibetan Plateau is modeled by applying a one-dimensional heat transfer model with phase change. The two main forcing variables are surface air temperature, from the ERA-40 reanalysis, and snow depth, derived from passive microwave satellite data. Daily fields of soil temperature are simulated, ranging from the soil surface down to 30 m depth, and the horizontal grid cell resolution is 25 km × 25 km. Results are presented for three different soil moisture regimes. The trend analysis is based on daily fields of active-layer depth (ALD) for the period January 1980 through December 2001. Significant positive ALD trends for all Tibetan permafrost regions are simulated in response to positive air temperature trends, with the strongest trend for the northern Tibetan Plateau (+1.4 cm yr^{-1}). Significant trends can reach +4 cm yr^{-1} locally. The day of year when ALD was reached shows strong interannual variation, and significant trends occur for smaller areas than for ALD. As an application, the active-layer deepening is presented along the tracks of the Qinghai-Tibet railroad line that has recently been completed.

Introduction

Soil temperature is a sensitive climate indicator and integrator, and plays an important role in the physical and biological processes that occur in soil. It is a valuable parameter for monitoring climate change because it integrates all processes occurring at and above the ground surface, such as air temperature, precipitation, snowfall, seasonal snow cover, vegetation, and surface microrelief, as well as the effects of soil type, soil moisture, and freezing and thawing processes. Increases in air temperature have a positive impact on soil temperature. Increased snowfall in early winter will have a strong positive impact on the soil thermal regime, whereas late snowfall may have a negative impact due to its high albedo and consumption of latent heat during snowmelt (Zhang et al., 2001a; Zhang, 2005a). In areas of ice-rich permafrost, warming and thawing of permafrost due to climate change will result in instabilities in the landscape and changes to the engineering behavior of soils, with direct impacts on ecosystems, communities, and infrastructure (Nelson et al., 2001).

Knowledge of baseline permafrost thermal conditions is essential to monitoring and assessing changes in permafrost. This is important for assessing natural or human-induced climate change and for impact and adaptation studies, and is critical for land-use planning and infrastructure design, construction, operation, and maintenance. Because of the potential response of the ground thermal regime, especially the seasonal freeze/thaw cycle and permafrost in cold regions, to predicted global warming, it is critical to understand the linkage between subsurface soil temperature and environmental factors. One major obstacle for assessing changes in the soil thermal regime is the lack of long-term observations of soil temperature and related climate variables (Zhang et al., 2001b).

Regions underlain by permafrost have been reduced in extent over the past decades (Anisimov et al., 2001). Climate models predict that, mainly due to the snow/ice-albedo feedback, warming will be amplified in high-latitude regions (Cubasch et al., 2001; Serreze et al., 2000), as well as over the Tibetan Plateau (Qin, 2002). Anisimov and Nelson (1997) simulated the reduced permafrost distribution in the Northern Hemisphere for the decade around 2050, based on different climate scenarios from GCMs.

Climate warming may cause large areas of permafrost in the −2°C to 0°C range to disappear, even if buffer factors such as snow, vegetation, and organic cover act to reduce the impact increases in air temperature have on the ground temperature (Smith and Burgess, 1999; Zhao et al., 2000). For northwestern Siberia, Pavlov and Moskalenko (2002) reported a more pronounced response of permafrost temperature to climate warming than the response of soil seasonal thawing, primarily due to changes in the snow insulation effect. They also described a cooling effect of shallow ground vegetation on soil during early summer and a resulting delay in the onset of thawing.

Oelke et al. (2003) and Oelke and Zhang (2003) modeled daily thaw depth for two complete freezing and thawing seasons over the Arctic drainage basin and compared their results to measurements taken at Circumpolar Active Layer Monitoring (CALM) field sites (Brown et al., 2000; Hinkel and Nelson, 2003). Modeled and measured thaw depths agree quite well, although there remain scale issues between the coarser model results and point measurements not representative of larger areas.

Jin et al. (2000) and Zhang (2005b) provided a detailed overview of permafrost research in China. A number of permafrost studies on the Tibetan Plateau have been conducted over the past several decades (Zhou and Du, 1963; Zhou, 1965; Wang et al., 1979; Cheng, 1982, 1997; Cheng and Wang, 1982; Tong and Li, 1983; Zhou et al., 2000; Zhao et al., 2000, 2004). Here we give a brief discussion of specific permafrost investigations on the Tibetan Plateau.

The majority of the Tibetan Plateau is above 4000 m a.s.l. (Fig. 1), with altitude being the primary control on permafrost development over the study area. Permafrost regions over the Tibetan Plateau occupy about 1.5 × 10^6 km^2, or approximately

1523-0430/07 $7.00

70% of the permafrost regions in China (Tong and Li, 1983; Zhou et al., 2000). Based on data and information from the International Permafrost Association's (IPA) Circum-Arctic Map of Permafrost and Ground Ice Conditions (Brown et al., 1997) and the Map of Geocryological Regionalization and Classification in China (Qiu et al., 2000), the Tibetan Plateau is dominated by discontinuous and sporadic permafrost. Permafrost temperatures at the depth of zero annual amplitude are in general above −5°C, with the majority being between 2 and 3°C below the freezing point (Tong and Li, 1983; Zhou et al., 2000). In this case, permafrost is very sensitive to thaw resulting from surface disturbance or climate warming. Recent studies indicate that along the Qinghai-Tibet (Xizang) highway, permafrost temperatures have increased by about 0.5 to 0.7°C from the 1970s to 2002 (Zhao et al., 2000, 2004; Wu and Liu, 2004). The thickness of the active layer has increased by up to 1.0 m along the highway from the 1980s to the early 1990s (Wu and Tong, 1995), with an additional increase of 0.25 to 0.60 m observed from the mid-1990s to the early 2000s (Zhao et al., 2004; Wu and Liu, 2004). Observed evidence indicates that the areal extent of permafrost islands from Amdo to Liangdaohe along the Qinghai-Xizang highway has decreased by 35.6% (Wang, 2002). The depth of the lower permafrost boundary under the northern Plateau has risen up by 25 m in the past three decades (Nan et al., 2003). Present permafrost thickness varies from a few meters to over 300 m on the Tibetan Plateau (Zhou et al., 2000).

It is predicted that mean annual surface air temperature will increase by 2.2 to 2.6°C by 2050 over the Tibetan Plateau (Qin, 2002). The potential impact of this warming on the ground thermal regime and permafrost conditions would be substantial. The Qinghai-Xizang railroad crosses 550 km of permafrost, of which 50% is high-temperature permafrost and 37% is ice-rich permafrost (Cheng, 2005). The construction and future operation of the railroad would have a great impact on local and regional environments and climate, and hence on the active layer and permafrost conditions. Understanding the response of the active layer and permafrost to changes in climate and surface disturbance due to human activities is a prerequisite for assessing regional ecosystem/environmental change and the effects of industrial development.

Permafrost studies on the Tibetan Plateau go back to the late 1950s, however, the majority of the work was focused along the Qinghai-Xizang highway. The Plateau permafrost distribution map compiled by Li and Cheng (1996) was mainly based on data and information from the map (1:600,000) (Wang et al., 1979) of permafrost distribution along the Qinghai-Xizang highway.

In this study, we simulate the soil thermal regime on a daily basis at 25 km × 25 km resolution for the Tibetan Plateau and adjoining areas. Using daily modeled values for the entire Tibetan Plateau, we show for the first time fields of (1) active-layer depth (ALD)—maximum annual thaw depth—and (2) the timing when the active-layer depth is reached within the thawing season. Forcing variables for the thermal soil model include daily surface air temperature and snow depth, used together with static fields of soil moisture content, soil bulk density, and soil type at different depths, and snow density.

Methodology

In the following, we characterize the Tibetan Plateau in terms of geographic area and permafrost properties, describe the thermal soil model applied, and explain the input parameters used to drive this model.

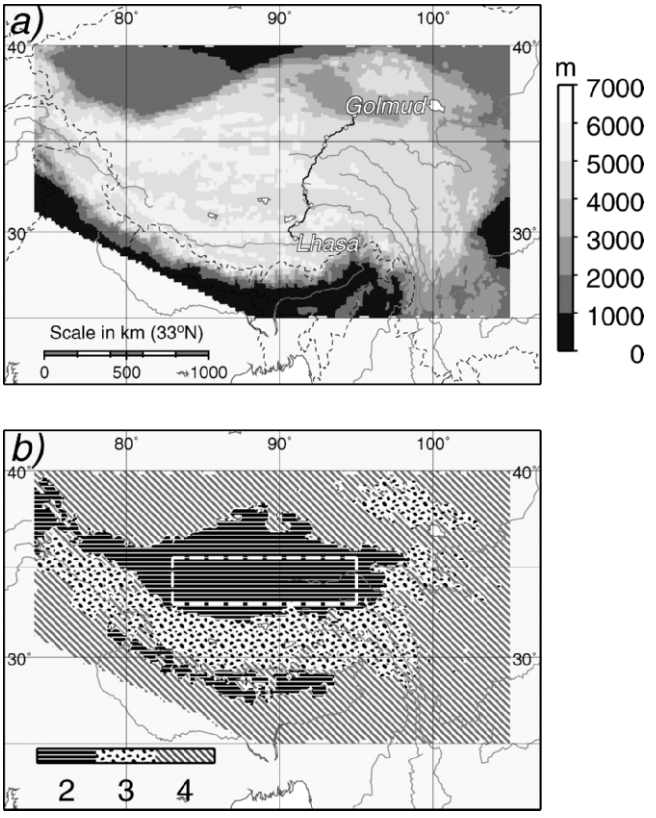

FIGURE 1. (a) Elevation map of the Tibetan Plateau model domain, including the location of the Qinghai-Tibetan railroad line (Golmnd to Lhasa). (b) Different patterns show the classification of the area by discontinuous [2], sporadic/isolated permafrost [3], and seasonally frozen ground [4]. Permafrost boundaries are based on the map by Brown et al. (1997). Also plotted are major rivers and political boundaries. The dashed rectangle denotes a northern subregion.

Study Area

The area of our simulations (Fig. 1) is defined in terms of nodes of the National Snow and Ice Data Center (NSIDC) north polar Equal-Area Scalable Earth (EASE) grid (Armstrong and Brodzik, 1995). The study area covers the discontinuous permafrost regions of the Tibetan Plateau and the high Himalaya as well as the sporadic and isolated permafrost areas south thereof and in the Altai mountain range. 963,936 km^2 or 22.1% of the area of the Tibetan model domain is underlain by discontinuous permafrost (black shaded areas in Fig. 1b, labeled 2), as defined by the IPA (Brown et al., 1997; IPA, 2003; Zhang et al., 1999). A further 19.3% (842,030 km^2) is classified as sporadic/isolated permafrost (labeled 3). Non-permafrost or seasonally frozen ground areas make up the remaining 58.6% (labeled 4). There are no regions classified as continuous permafrost like in the High Arctic. Our study area encompasses 21.8% of all discontinuous permafrost regions of the Northern Hemisphere and 10.6% of all sporadic/isolated permafrost regions. It covers 7.7% of all of the Northern Hemisphere's permafrost areas, and 14.6% of all discontinuous or sporadic/isolated permafrost regions.

Thermal Soil Model

We use a finite difference model for one-dimensional heat conduction with phase change (Goodrich, 1982). This model has been shown to provide excellent results for soil temperatures and

active-layer thickness (Zhang et al., 1996; Zhang and Stamnes, 1998) when driven with well-defined boundary conditions and forcing variables at specific locations. A detailed description of the model is given by Goodrich (1982) and Zhang et al. (1996), and only a brief summary is included here. A complete description of the model setup for circum-Arctic studies is given by Oelke et al. (2003), where the following simplifications are used: (1) the snow surface temperature is set equal to air temperature, (2) heat transfer is by conduction only within the snow layer, and (3) snow densities (see next section) are climatological. Our intent is to model soil temperature for the entire Tibetan Plateau and derive ALD. We run the model one dimensionally and assume no lateral heat transfer among the 25 km × 25 km grid cells.

Soil is divided into three major layers (0–30 cm, 30–80 cm, and 80–3000 cm), with distinct thermal properties for frozen and thawed soil, respectively. Calculations are performed on 63 model layers ranging from a thickness of 10 cm for the top 80 cm of soil, to 2 m at 30 m depth, the lower model boundary.

We prescribed an initial geothermal heat flux for every grid cell using a temperature gradient of 3°C per 100 m. We then ran the model with this condition for 20 years (1980 forcing) and used the resulting temperature gradient between the two lowest model layers, together with the bottom layer thermal conductivity, to calculate the new and spatially variable geothermal heat flux. This heat flux is almost negligible for the near-surface active layer, but it is more important to use realistic values at depths below the zero annual amplitude.

We chose initial soil temperatures according to the permafrost classification of the grid cell based on the IPA circumpolar map of permafrost and ground ice conditions on the NSIDC EASE-Grid (Brown et al., 1997; IPA, 2003; Zhang et al., 1999). In areas of discontinuous permafrost, the model was initialized for the first day of the simulation (1 January 1980) to −5°C on all layers, and the corresponding value for sporadic/isolated permafrost regions was −3°C. A value of +6°C was used for seasonally frozen ground regions. The model was spun up for 24 years using daily temperature and snow data of 1980 to obtain steady-state initial conditions for temperatures at all model layers. Calculations were then performed with a daily time step for the 22-year period from 1 January 1980 to 31 December 2001.

Model Forcing Parameters

The main forcing variables for the thermal soil model are surface air temperature and snow depth. We use 2 m surface air temperatures (Fig. 2a) from the European Centre for Medium-Range Weather Forecasts (ECMWF) ERA-40 reanalysis that is currently available until 31 August 2002. ERA-40 daily 2 m air temperatures (N80 resolution, regridded to 25 km × 25 km EASE-Grid from the original 1.125° lat × 1.125° long grid) were obtained from the ECMWF Web site (http://www.ecmwf.int). Frauenfeld et al. (2005) compared air temperature measurements from meteorological stations on the Tibetan Plateau to ERA-40 2 m temperatures. They concluded that the ERA-40 temperatures provide better spatial fields of the near-surface temperature than is possible with stations in this topographically complex, data sparse area. In addition, spatial fields are less influenced than station data by the extensive land-use change and industrialization that has occurred on the Tibetan Plateau. These conclusions provide confidence that ERA-40 daily 2 m air temperature is appropriate for this model study.

Snow water equivalent (SWE) was derived from passive microwave radiometer data from the Scanning Multichannel Microwave Radiometer (SMMR, 1980–1987) (Chang et al., 1987) and from the Special Sensor Microwave/Imager (SSM/I, 1987–2001) (Armstrong and Brodzik, 2001). SWE values (kg m^{-2}) are divided by a climatological snow density (kg m^{-3}) to derive snow depth (m) at the given location and time of year. These snow densities are obtained from a 45-year time series of Canadian snow data (1955–1999) (MSC, 2000) to define the climatological seasonal cycles of snow density for five specific regions from tundra to mountains (Oelke et al., 2003). The global snow-class regions were defined by Sturm et al. (1995) based on climatological values of temperature, precipitation, and wind speed. We will use snow-density measurements from the Tibetan Plateau if such climatologies should become available in the future.

Very thin snow cover often cannot be detected by passive microwave remote sensing. Therefore, we also used the EASE-Grid version of the NOAA-NESDIS weekly snow charts (Armstrong and Brodzik, 2002) for snow identification. The NOAA charts are based on information from several visible-band satellites. For grid cells where the SSM/I does not detect snow but the NOAA charts do, following Oelke and Zhang (2004), we assume a snow depth of 3 cm (dark gray areas in Fig. 2b). Snow thermal conductivity was calculated using a density-dependent formulation published by Sturm et al. (1997) that is based on regression through measurements over the past 100 years.

Further static model input parameters include soil bulk density and the relative compositions of fine-grained (clay/silt) and coarse-grained (sand/gravel) material (Global Soil Data Task, 2000) for each of the three major model layers. These were used to calculate soil thermal conductivity for the frozen and thawed states according to Kersten's (1949) formulations, modified by the thermal conductivity of peat with a density of 500 kg m^{-3} (De Vries, 1963) for up to 80 cm of soil (Oelke et al., 2003). Since spatial fields of soil water content are not available for this region, we perform sensitivity studies with a standard, dry, and moist case (Table 1).

Results and Analysis

SEASONAL AND INTERANNUAL ALD VARIATION

The soil thermal model with standard soil moisture is applied to every grid cell of our model domain and run for the time period 1980 through 2001 with a daily time step. Maps of resulting thaw depth for the whole Tibetan Plateau and on four days that illustrate the seasonal cycle (1 March, 1 June, 1 September, and 1 December 2000) are presented in Figure 3. In addition, values for sporadic permafrost grid cells that are not generally completely underlain by permafrost (i.e., between the Himalaya and the northern Plateau, cp. Fig. 1b) are shown here. A strong seasonal thaw depth cycle is obvious in Figures 3a–3d. Only the southernmost regions experience thawing as early as 1 March, whereas larger regions in southwestern Tibet have started thawing by 1 June. The ALD or annual maximum thaw depth is mostly reached in September. Thaw depth on 1 September 2000 reaches values of up to 2.5 m over isolated permafrost in southern Tibet, and between 0.5 m and 1.3 m over discontinuous permafrost on the northern high Plateau. Parts of southern and southeastern Tibet do not completely freeze up until 1 December, likely due to the effect of snow cover insulation. Thaw depth at the boundary between permafrost and non-permafrost regions is possibly contaminated by the lower-resolution temperature forcing or due to spotty permafrost distribution in the marginal regions.

ALD can vary by more than 20% from year to year, in response to the temperature and snow forcing. Figure 4 shows the

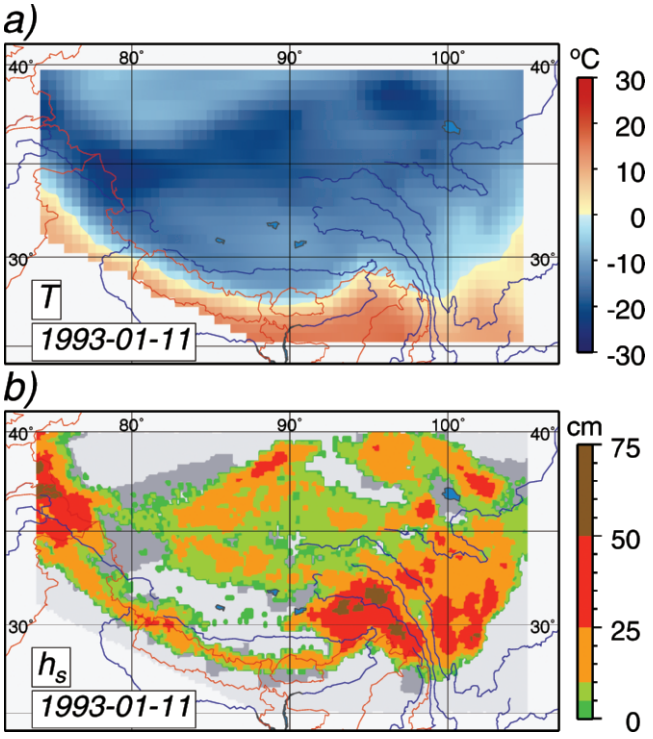

FIGURE 2. Example of model forcing for 11 January 1993: (a) ERA-40 2 m surface temperature *T*, and (b) snow height (thickness) *h* derived from passive microwave satellite data. Dark gray areas in (b) mark shallow snow regions that are only tracked by the NOAA charts (see text).

comparison between ALD of two extreme years within our time series, namely 1984 and 1998. ALD in 1998 in south-central Tibet is up to 2.8 m, and larger areas of the northern Plateau show thawing of more than 1 m (green shading).

The climatological ALD for the 22 years from 1980 to 2001 is shown in Figure 5a. Values of the high western Plateau are below 1 m, and values in the northern subregion range between 0.5 m and 1.5 m. The sporadic and isolated permafrost regions of south-central Tibet show average ALDs between 2 m and 3 m. Since permafrost here often does not cover a complete grid cell, a likely too warm forcing climate (for the permafrost fraction of the grid cell) may produce artefacts. A larger area with higher standard deviation (0.05 m to 0.10 m) is obvious for the northwestern Plateau (Fig. 5b) and can be associated with regions of larger significant ALD deepening trends.

Similarly, the date when ALD is reached within one year (Day [ALD]) also shows considerable interannual variation (1986 and 1998 in Fig. 6). Later refreezing in the year implies longer and stronger summer thaw seasons, leading to higher ALD. The

TABLE 1

Degree of soil moisture saturation of the three main model layers (dependent on soil bulk density or porosity) and for three considered cases.

Layer	Dry case	Standard case	Moist case
0–30 cm	85%	99%	99%
30–80 cm	75%	85%	95%
Below 80 cm	60%	70%	90%

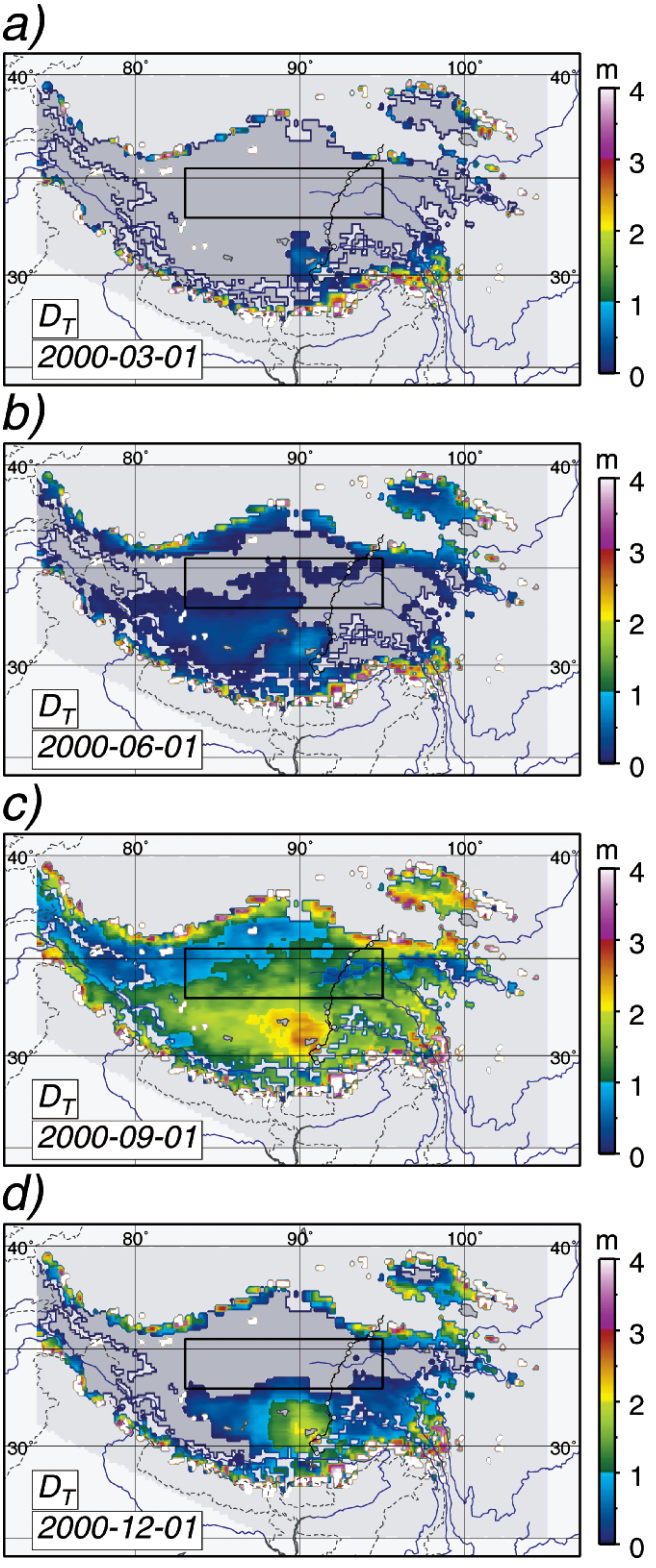

FIGURE 3. Illustration of the annual thaw depth cycle by daily fields in three-month intervals: (a) 1 March, (b) 1 June, (c) 1 September, and (d) 1 December. A rectangle marking the northern subregion, and the location of the Qinghai-Tibet railroad line are also included.

maximum annual thaw depth is reached by 1 September on the northern Plateau (day 250). Thawing until late October (day 300) can occur in the southern regions, but the actual dates can vary by three weeks between extreme years.

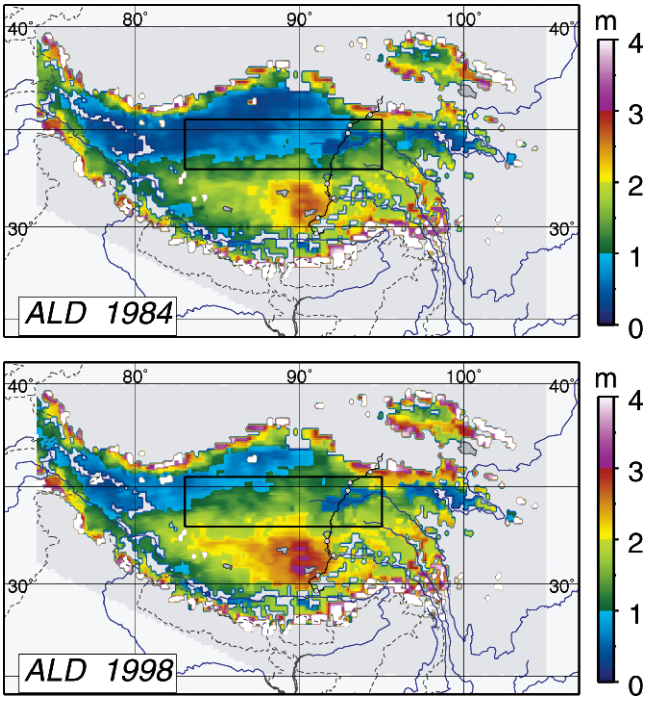

FIGURE 4. Simulated active-layer depth (ALD) for all Tibetan Plateau permafrost regions in two extreme years (1984 and 1998, cp. to the time series of Fig. 7a).

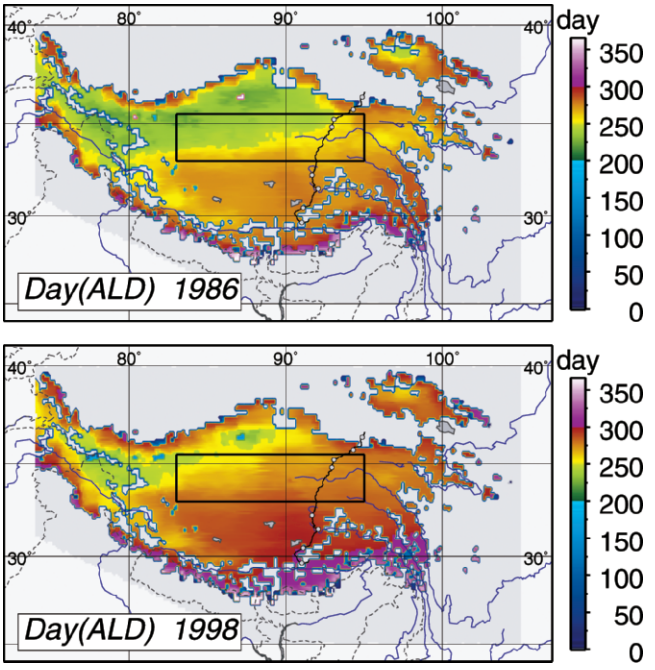

FIGURE 6. The day when the active-layer depth (ALD) was reached (Day [ALD]) in two extreme years (1986 and 1998, cp. to the time series of Fig. 7b).

TREND ANALYSIS, 1980–2001

Here we present results from a trend analysis of ALD, covering our model period from 1980 to 2001. We divided our domain into three subsets in order to be able to make more regional assessments. The first subset covers the discontinuous permafrost region (cp. Fig. 1), and the second one covers the sporadic permafrost region. We also show results for the rectangular region in northern Tibet that covers large parts of those discontinuous permafrost areas.

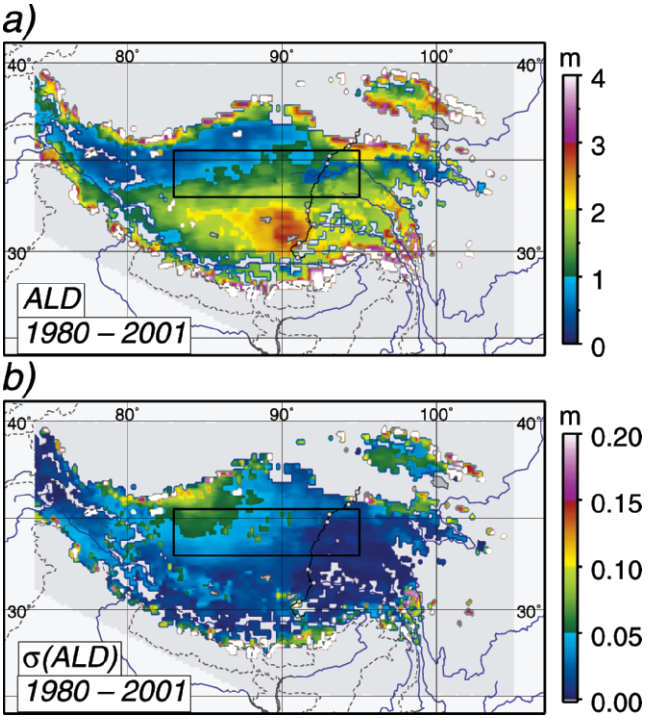

FIGURE 5. (a) Average active-layer depth (ALD) for the years 1980–2001, and (b) its standard deviation σ(ALD).

ALD in all three subregions increases over the observation period (Fig. 7a). Average ALDs in discontinuous permafrost regions increase from ~1.2 m to ~1.5 m, in sporadic permafrost regions from ~1.7 m to ~1.9 m, and in the northern subregion from ~1.0 m to ~1.3 m. The shading refers to the average ALD of these three regions. Averages are lowest in the northern subregion, with 1.14 m, followed by averages in discontinuous (1.44 m) and in sporadic permafrost regions (1.79 m). Trends of rate of change in ALD are largest for the northern subregion, with 1.38 cm yr^{-1}, followed by 1.23 cm yr^{-1} for the discontinuous permafrost regions. These trends are significant at the 99% confidence level. Trends in sporadic permafrost regions are 0.66 cm yr^{-1} and significant at the 95% confidence level. Studies of ALD trends in the Arctic (Oelke et al., 2004) found large, significantly positive trends for southern Alaska, northern Canada, and south-central Siberia of the same order of magnitude (1–5 cm yr^{-1}) as presented in this study.

The trends are virtually independent of the soil moisture content (Table 1), and calculated ALDs vary in the range of 10 to 14 cm between the extreme moisture cases (long dashed and short dashed curves in Fig. 7). Higher soil moisture content increases soil thermal conductivity, resulting in slightly higher ALDs. Yang et al. (2003) demonstrated from site measurements along the Qinghai-Tibetan highway that soil moisture can be important for freezing and thawing processes, and that soil layers with higher moisture content can exist below dryer layers (unlike our standard soil moisture profile.) But calculations with our model for a modified standard case (with 85% saturation for the top soil layer, 99% for the middle soil layer, and 70% below) yield almost unchanged ALDs with respect to the standard case ($\Delta ALD <$ 2 cm for annual averages of the three regions.) These variations in ALDs are much smaller compared to those for the extreme moisture cases (moist, dry).

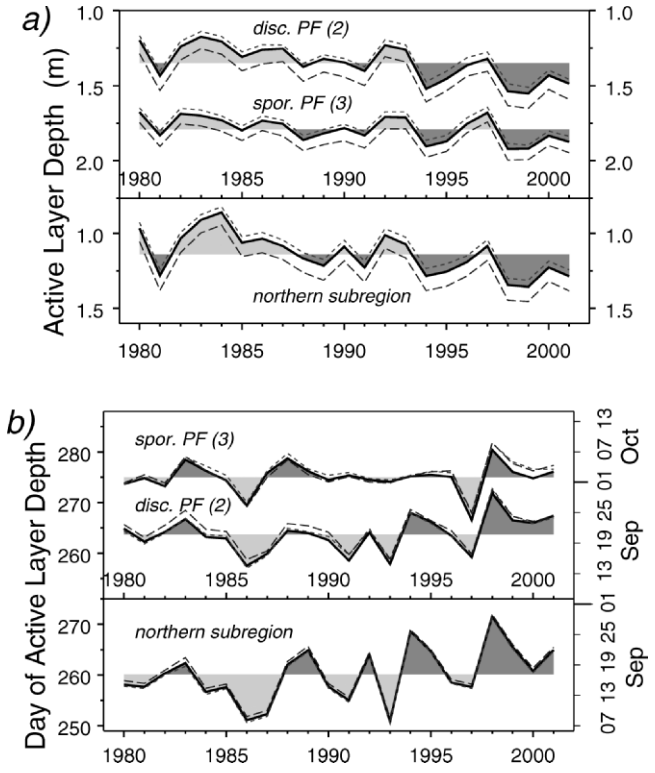

FIGURE 7. (a) Time series of active-layer depth (ALD), 1980–2001, for discontinuous [2] and sporadic permafrost [3], as well as for a subregion in northern Tibet. The dark gray and light gray shading refers to the average of the time series. Results for low (short-dashed lines) and high soil moisture content (long-dashed lines) are plotted for comparison. (b) Same as (a), but for the day when the ALD was reached within the particular year.

A time series of the day of year when ALD was reached within each year is presented in Figure 7b for the same three regions as for ALD. The average day of year in the northern subregion is day 260 (17 September), in discontinuous permafrost regions day 264 (21 September), and in sporadic permafrost regions day 275 (2 October). But year-to-year variations of this day are large. They can be up to two weeks in sporadic permafrost regions (standard variation $\sigma = 2.8$ days), and up to three weeks in the northern subregion ($\sigma = 5.4$ days). Consequently, even the largest calculated trend for day of year (0.35 days yr^{-1} for the northern subregion) is insignificant at the 95% confidence level. Soil moisture content seems to play a less important role in the timing of the ALD than it plays for determining its maximum value (Fig. 7).

To examine the spatial patterns of ALD changes in more detail, we calculate linear trends of the 22-year time series for every model grid cell. ALD trends for all permafrost regions within our domain that are significant at the 95% confidence level are presented in Figure 8a. Almost all significant trends of the Tibetan domain are positive. Large portions of the northern discontinuous permafrost regions (cp. to Fig. 1b) reveal significant positive trends of 1 to 3 cm yr^{-1}. The areas with significant ALD trends in the order of 2 to 4 cm yr^{-1} for the northwestern Plateau correspond to regions of higher standard deviation ($\sigma = 0.04$–0.14 m) (Fig. 5b).

Simulated trends in ALD compare well spatially to trends in ERA-40 surface temperature. Following the analysis and procedure of Frauenfeld et al. (2005) for 1958–2000, monthly temperature trends were calculated for all ERA-40 grid cells on the Tibetan Plateau for the period 1980–2000 (O. Frauenfeld, 2006, personal communication). Grid cells centered at 35°N, and between 77.5°E and 90°E, experience warming trends of 0.8 to 1.3°C per decade. Trends are significant at the 95% confidence level for the months May, June, July, and September—except for August, the months most important for the development of the ALD over frozen soil. Our ALD trends are largest here (roughly the area of the northern subregion, Fig. 8a), with 1–3 cm yr^{-1}. ERA-40 temperature trends north thereof (centered at 37.5°N, between 85°E and 90°E) are only significant for June and September, whereas trends to the south (centered at 32.5°N, between 85°E and 90°E) are only significant for May and November. Winter trends (December through April) are generally insignificant.

Only the westernmost portions and the parts east of the Qinghai-Tibet railroad line show no significant trends. Ground-based measurements along the Qinghai-Xizang highway reveal that active-layer thickness has increased significantly from the early 1980s to 2002, in some cases by up to 1.0 m (Wu and Tong, 1995; Zhao et al., 2004). Wu and Liu (2004) report measured trends for 1995–2002 between 0.8 and 8.4 cm yr^{-1} for sites on the northern part of the Plateau along the highway. At our relatively coarse grid-cell resolution, we model long-term significant trends of between 0.5 and 2 cm yr^{-1} for these regions (Fig. 8a), but increased trends in the range of 3 to 5 cm yr^{-1} between the mid-1990s and 2001.

A positive 22-year trend in the day of year when the ALD is reached is due to an increase in the length of thawing season. Here, the ALD is continually reached later in the year. The regions that show a significantly positive trend of Day (ALD) are smaller than those that experience a significant ALD increase. We can refine the findings of insignificant Day (ALD) trends when averaged over larger regions (Fig. 7b) by mapping the locations of grid cells that in fact show significant positive trends (Fig. 8b). The trends are mostly between 0.25 and 1 day yr^{-1}.

QINGHAI-TIBET RAILROAD LINE

For construction projects it can be important to assess ALD and its variability for specific locations. The Qinghai-Tibet railroad line has led as far west as Golmud in Qinghai province. It has been extended into Tibet (Fig. 9a), with Lhasa as the final station, and was completed in July 2006. A total length of tracks of 1080 km was built, with 960 km running at altitudes of more than 4000 m, and Tanggula Pass being the highest point, with an elevation of 5072 m. Large portions lead through frozen ground or permafrost areas that are susceptible to soil warming. Soil instability and potential hazards to construction and operation will result from permafrost thawing and the deepening of the active layer.

Modeled average ALD, standard deviation, and minimum/maximum values along the railroad line from Golmud (left) to Lhasa (right) is shown in Figure 9c. The high Plateau areas southwest of Wudaoliang are characterized by ALDs of about 0.5 m and little interannual variation. ALDs of the adjacent areas north and south thereof range between 1 and 3 m, with variations of more than 0.5 m between the years. Later years produce the largest ALDs with differences between the average ALD of 1991 to 2001 and the average ALD of 1980 to 1990 being mostly positive (up to 0.18 m). This supports the findings of the previous sections, with soil warming and active-layer deepening over these 22 years (see Fig. 7). A significant ALD increase is only evident

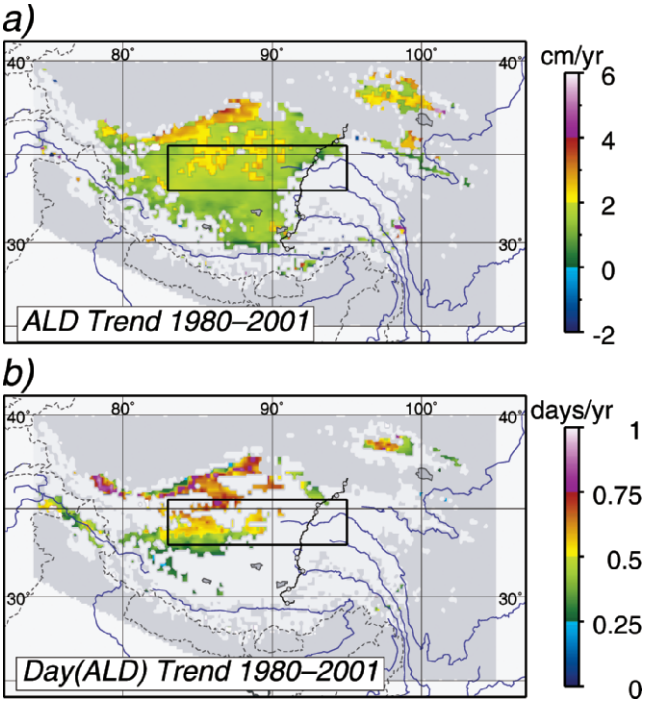

FIGURE 8. (a) Map of active-layer depth (ALD) trends (1980–2001) that are significant at the 95% confidence level. Trends in light gray areas are not significant. (b) Significant trends in the timing of when the active-layer depth is reached within the year (Day [ALD]).

for the northernmost permafrost regions along the railroad line (north of Bailuhe) on the north slope of the Plateau (Fig. 8a). The railroad line currently seems to lie outside of regions with the largest trends, but interannual variations of ALD may still pose a risk to construction.

Year-to-year variation in the day of year when ALD is reached is large (Fig. 9d). Maxima on the high Plateau are reached between mid- and late September, whereas they can be as late as mid-October for the other areas. Differences between the averages of 1991 to 2001 and 1980 to 1990 are positive for the northern part of the railroad line, with up to 4.3 days, whereas they are around zero for most of the southern part of the line. Only for a small portion between Wudaoliang and Xidatan, the ALD is reached significantly later in the year over the 22-year period (cp. Fig. 8b).

The model results generally agree with the ranges of measured ALD given by Zhou et al. (2000) for the Xidatan to Kunlun Mountains area, and for the Tanggula Mountains to Liangdaohe area. A somewhat larger range in ALD may be due to interannual variation of the soil moisture content and sub-grid cell features in the temperature and snow forcing. The measurements for the Yangtse River source area (kilometers 240–340 in

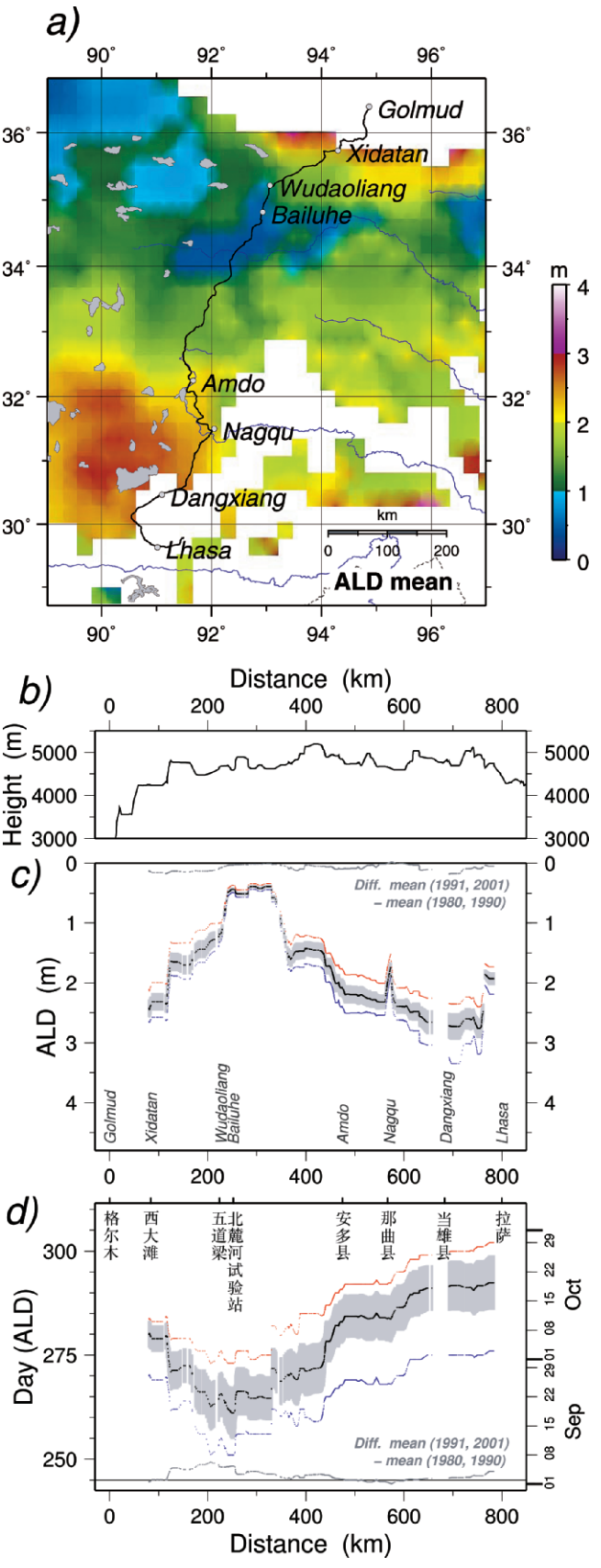

FIGURE 9. (a) Location of the Qinghai-Tibet (Xizang) railroad line that was completed in 2006. Underlain is the modeled climatological active-layer depth (ALD). Areas in light gray mark lakes. (b) Elevation a.s.l. along the railroad line (cp. Fig. 1a). (c) Modeled average ALD (black dots) over permafrost along the Qinghai-Tibet railroad line from Golmod (left) to Lhasa (right). The shading refers to ±1 standard deviation, and blue and red dots mark minimum and maximum values of the whole time series. Also plotted is the difference between the average ALD of the later part of the time series (1991–2001) and the average of the earlier part (1980–1990) (dots in the 0 to 0.2 m range). (d) Illustration of the variability in the day of year when the active-layer depth is reached (Day [ALD]) along the same route. The difference between the last 11 years of the time series and the first 11 years is plotted at the bottom (with 245 added to the values). Station locations along the railroad line are labeled in Latin (c) and Chinese characters (d).

Fig. 9c) are higher than the simulations that are in the 50 cm range. This is likely due to the fact that measurements are taken in the valleys, whereas the larger ERA-40 grid cells are based on spatial averages, including values from high elevations, and are therefore colder.

Conclusions

ALD of the whole Tibetan Plateau was modeled for the first time at daily time steps. A grid cell resolution of 25 km × 25 km was used, and reanalyzed surface air temperature and remotely sensed snow cover were the main forcing variables.

The analyzed 22-year time series (1980–2001) of ALDs reveals considerable interannual and spatial variation, with soil moisture slightly influencing the maximum value of thawing, but not its timing or trends. Soil warming trends are manifested in an average deepening of active layers by up to 1.38 cm yr^{-1} for the coldest and highest locations on the northern part of the Plateau. ALD trends can reach 2–4 cm yr^{-1} in some regions, which is comparable to the significant increase in ALD found for southern Alaska, northern Canada, and south-central Siberia (1–5 cm yr^{-1}). Though significant trends of ALD increase are smaller for sporadic permafrost regions (0.66 cm yr^{-1}), it is especially those relatively warm regions with soil temperatures in the −2 to 0°C range that are of greatest risk of thawing.

There are many factors influencing soil freezing and thawing processes, and therefore, the active-layer thickness. These factors include air temperature, seasonal snow cover, vegetation, surface wetness and soil moisture, and soil physical and thermal properties. Although the model used in this study has been validated for site-specific studies in the Arctic, forcing variables for model simulations are critical for regional-scale studies, especially over the Tibetan Plateau where ground-based measurements are sparse. With further improvements of data and information from in-situ measurements and satellite remote sensing, simulated results over the Tibetan Plateau will be improved significantly.

An expansion of the Circumpolar Active Layer Monitoring (CALM) network to more sites in discontinuous and sporadic permafrost regions, in particular to high altitude permafrost regions in the mid-latitudes (like the Tibetan Plateau), will greatly benefit modeling efforts in terms of input and validation for active layer and permafrost studies.

Acknowledgments

We thank Andrew Etringer of the National Snow and Ice Data Center (NSIDC), University of Colorado at Boulder, for preparing data sets. This study was supported by the U.S. National Science Foundation (NSF) under grants OPP-0352910, OPP-0229766, OPP-0328664, and ARC-0612431; the U.S. National Aeronautics and Space Administration (NASA) grants NAG5-13721, NNG04GJ39G, and NNX06AE65G; the Westfälische Wilhelms University, Münster, Germany; two travel grants of the German Research Foundation; the Chinese Academy of Sciences (CAS) International Partnership Project (CXTD-Z2005-2); and by the Chinese Academy of Meteorological Sciences, China Meteorological Administration (CMA). Financial support does not constitute an endorsement of the views expressed in this article.

References Cited

Anisimov, O. A., and Nelson, F. E., 1997: Permafrost zonation and climate change in the Northern Hemisphere: results from transient General Circulation Models. *Climatic Change*, 35: 241–258.

Anisimov, O., Fitzharris, B., Hagen, J. O., Jefferies, R., Marchant, H., Nelson, F., Prowse, T., and Vaughan, D. G., 2001: Polar regions (Arctic and Antarctic). *In* Climate change: impacts, adaptation and vulnerability. Contribution of Working Group II of the Intergovernmental Panel on Climate Change (IPCC), Third Assessment Review. Cambridge, UK: Cambridge University Press.

Armstrong, R. L., and Brodzik, M. J., 1995: An earth-gridded SSM/I data set for cryospheric studies and global change monitoring. *Advanced Space Research*, 16(10): 155–163.

Armstrong, R. L., and Brodzik, M. J., 2001: Recent Northern Hemisphere snow extent: a comparison of data derived from visible and microwave satellite sensors. *Geophysical Research Letters*, 28(19): 3673–3676.

Armstrong, R. L., and Brodzik, M. J., 2002: *Northern Hemisphere EASE-Grid weekly snow cover and sea ice extent, version 2*. Boulder, CO: National Snow and Ice Data Center, CD-ROM.

Brown, J., Ferrians, O. J. J., Heginbottom, J. A., and Melnikov, E. S., 1997: *International permafrost association circum-Arctic map of permafrost and ground ice conditions*. Washington, DC: U.S. Geological Survey, scale 1:10,000,000.

Brown, J., Hinkel, K. M., and Nelson, F. E., 2000: The Circumpolar Active Layer Monitoring (CALM) program: research designs and initial results. *Polar Geography*, 24(3): 163–258.

Chang, A. T. C., Foster, J. L., and Hall, D. K., 1987: Nimbus-7 SMMR derived global snow cover parameters. *Annals of Glaciology*, 9: 39–44.

Cheng, G. D., 1982: Formation mechanism of massive ground ice. *Science in China (B)*, 3: 281–287.

Cheng, G. D., 1997: *An assessment of climate change impact on snow cover, glacier, and permafrost in China*. Lanzhou, China: Gansu Culture Press, 108 pp. (in Chinese with English Table of Contents).

Cheng, G. D., 2005: A roadbed cooling approach for the construction of Qinghai-Tibet Railway. *Cold Regions Science and Technology*, 42: 169–176.

Cheng, G. D., and Wang, S. L., 1982: On the zonation of mountain permafrost in China. *Journal of Glaciology and Geocryology*, 4(2): 1–17.

Cubasch, U., Meehl, G. A., Boer, G. J., Stouffer, R. J., Dix, M., Noda, A., Senior, C. A., Raper, S., and Yap, K. S., 2001: Projections of future climate change. *In* Climate change: the scientific basis. Contribution of Working Group I of the Intergovernmental Panel on Climate Change (IPCC), Third Assessment Review. Cambridge, UK: Cambridge University Press.

De Vries, D. A., 1963: Thermal properties of soils. *In* Van Wijk, W. R. (ed.), *Physics of plant environment*. Amsterdam: North-Holland Publishing Co., 210–235.

Frauenfeld, O. W., Zhang, T., and Serreze, M. C., 2005: Climate change and variability using European Centre for Medium-Range Weather Forecasts reanalysis (ERA-40) temperatures on the Tibetan Plateau. *Journal of Geophysical Research*, 110: D02101, doi: 10.1029/2004/JD005230.

Global Soil Data Task, 2000, Global gridded surfaces of selected soil characteristics (IGBP-DIS). International Geosphere-Biosphere Programme—Data and Information Services. Oak Ridge, Tennessee: ORNL Distributed Active Archive Center, Oak Ridge National Laboratory, (http://www.daac.ornl.gov). Last accessed on 9 July 2007.

Goodrich, L. E., 1982: Efficient numerical technique for one-dimensional thermal problems with phase change. *International Journal of Heat and Mass Transfer*, 21: 615–621.

Hinkel, K. M., and Nelson, F. E., 2003: Spatial and temporal patterns of active layer thickness at Circumpolar Active Layer Monitoring (CALM) sites in northern Alaska, 1995–2000.

Journal of Geophysical Research, 108(D2): 8168, doi: 10.1029/2001JD000927.

IPA (International Permafrost Association), 2003, *Circumpolar Active-Layer Permafrost System (CAPS), Version 2.0*, M. Parsons, and T. Zhang (eds.), Standing Committee on Data Information and Communication (comp). Boulder, CO: National Snow and Ice Data Center/World Data Center for Glaciology, CD-ROM.

Jin, H. J., Cheng, G. D., and Zhu, Y. L., 2000: Chinese geocryology at the turn of the twentieth century. *Permafrost Periglacial Processes*, 11: 22–23.

Kersten, M. S., 1949: *Laboratory research for the determination of the thermal properties of soils: final report*. Hanover, N.H.: U.S. Army Corps of Engineers, Cold Regions Research and Engineering Laboratory, ACFEL Technical Report 23, 235 pp.

Li, S. D., and Cheng, G. D., 1996: *Permafrost map of the Qinghai-Xizang Plateau*. Lanzhou, China: Gansu Culture Press, scale 1:3,000,000 (in Chinese).

MSC (Meteorological Service of Canada), 2000, *Canadian Snow Data CD-ROM*. Downsview, Ontario: CRYSYS Project, Climate Processes and Earth Observation Division.

Nan, Z., Gao, Z., Li, S., and Wu, T., 2003: Permafrost changes in the northern limit of permafrost on the Qinghai-Tibetan Plateau in the past 30 years. *Acta Geographica Sinica*, 58(6): 817–823. (in Chinese).

Nelson, F. E., Anisimov, O. A., and Shiklomanov, N. I., 2001: Subsidence risk from thawing permafrost. *Nature*, 410(6831): 889–890.

Oelke, C., and Zhang, T., 2003: Comparing thaw depths measured at CALM field sites with estimates from a medium-resolution hemispheric heat conduction model. *In* Extended Abstracts of the 8th International Conference on Permafrost, Zürich, Switzerland, 117–118.

Oelke, C., and Zhang, T., 2004: A model study of circum-Arctic soil temperatures. *Permafrost and Periglacial Processes*, 15(2): 103–121.

Oelke, C., Zhang, T., Serreze, M. C., and Armstrong, R. L., 2003: Regional-scale modeling of soil freeze/thaw over the Arctic drainage basin. *Journal of Geophysical Research*, 108(D10): 4314, doi: 10.1029/2002JD002722.

Oelke, C., Zhang, T., and Serreze, M. C., 2004: Modeling evidence for recent warming of the Arctic soil thermal regime. *Geophysical Research Letters*, 31(7): L07208, doi: 10.1029/2003GL019300.

Pavlov, A. V., and Moskalenko, N. G., 2002: The thermal regime of soils in the north of western Siberia. *Permafrost and Periglacial Processes*, 13: 43–51.

Qin, D. H., 2002: *Assessment of environmental changes in western China*. Beijing, China: Science Press.

Qiu, G. Q., Zhou, Y. W., Guo, D. X., and Wang, Y. X., 2000: *The map of geocryological regionalization and classification in China*. Xian, China: Xian Press, scale 1:10,000,000 (in Chinese and English).

Serreze, M. C., Walsh, J. E., Chapin, F. S. III, Osterkamp, T., Dyurgerov, M., Romanovsky, V., Oechel, W. C., Morison, J., Zhang, T., and Barry, R. G., 2000: Observational evidence of recent change in the northern high-latitude environment. *Climate Change*, 46: 159–207.

Smith, S. L., and Burgess, M. M., 1999: Mapping the sensitivity of Canadian permafrost to climate warming. *In*Interactions between cryosphere, climate and greenhouse gases. Proceedings of the IUGG 99 Symposium HS2, Birmingham. *IAHS Publication*, 256: 71–80.

Sturm, M., Holmgren, J., and Liston, G. E., 1995: A seasonal snow cover classification system for local to global applications. *Journal of Climate*, 8(5): 1261–1283.

Sturm, M., Holmgren, J., König, M., and Morris, K., 1997: The thermal conductivity of seasonal snow. *Journal of Glaciology*, 43(143): 26–40.

Tong, B., and Li, S., 1983: *Characteristics and controlling factors of permafrost on the Qinghai-Xizang (Tibetan) Plateau, special issue on permafrost research on the Qinghai-Xizang Plateau, Lanzhou Institute of Glaciology and Geocryology, Chinese Academy of Sciences*. Beijing: Science Press, 1–11 (in Chinese with English abstract).

Wang, J. C., Wang, S. L., and Qiu, G. Q., 1979: Permafrost along the Qinghai-Xizang Plateau. *Journal of Geography*, 34(1): 18–32.

Wang, S., 2002: Chapter 8, Permafrost degradation, desertification, and CH4 release. *In* Dynamic characteristics of cryosphere in the central part of the Qinghai-Xizang Plateau. Beijing: Geology Press, 234–255. (in Chinese).

Wu, Q., and Liu, Y., 2004: Ground temperature monitoring and its recent change in Qinghai-Tibetan Plateau. *Cold Regions Science and Technology*, 38: 85–92.

Wu, Q., and Tong, C., 1995: Change of the permafrost and stability along the Qinghai-Xizang Highway. *Journal of Glaciology and Geocryology*, 17(4): 350–355, (in Chinese with English Abstract).

Yang, M., Yao, T., Gou, X., Koike, T., and He, Y., 2003: The soil moisture distribution, thawing-freezing processes and their effects on the seasonal transition on the Qinghai-Xizang (Tibetan) Plateau. *Journal of Asian Earth Sciences*, 21(5): 457–465.

Zhang, T., 2005a: Influence of the seasonal snow cover on the ground thermal regime: an overview. *Reviews of Geophysics*, 43: 1–23, RG4002, doi:10.1029/2004RG000157.

Zhang, T., 2005b: Historical overview of permafrost studies in China. *Physical Geography*, 26(4): 279–298.

Zhang, T., and Stamnes, K., 1998: Impact of climatic factors on the active layer and permafrost at Barrow, Alaska. *Permafrost and Periglacial Processes*, 9: 229–246.

Zhang, T., Osterkamp, T. E., and Stamnes, K., 1996: Influence of the depth hoar layer of the seasonal snow cover on the ground thermal regime. *Water Resources Research*, 32(7): 2075–2086.

Zhang, T., Barry, R. G., Knowles, K., Heginbottom, J. A., and Brown, J., 1999: Statistics and characteristics of permafrost and ground-ice distribution in the Northern Hemisphere. *Polar Geography*, 23(2): 132–154.

Zhang, T., Barry, R. G., and Haeberli, W., 2001a: Numerical simulations of the influence of the seasonal snow cover on the occurrence of permafrost at high latitudes. *Norwegian Journal of Geography*, 55(4): 261–266.

Zhang, T., Barry, R. G., Gilichinsky, D., Bykhovets, S. S., Sorokovikov, V. A., and Ye, J., 2001b: An amplified signal of climatic change in soil temperatures during the last century at Irkutsk, Russia. *Climatic Change*, 49: 41–76.

Zhao, L., Chen, G., and Cheng, G., 2000: Chapter 6: Permafrost: status, variation, and impact. *In* Du Zheng., and Qingsong. (eds.), *Mountain geoecology and sustainable development of the Tibetan Plateau*. Beijing: Science Press, 134–147.

Zhao, L., Ping, C., Yang, D., Cheng, G-D., Ding, Y., and Liu, L., 2004: Changes of climate and seasonally frozen ground over the past 30 years in Qinghai-Xizang (Tibetan) Plateau, China. *Global and Planetary Changes*, 43: 19–31.

Zhou, Y., 1965: *Permafrost along the Qinghai-Xizang Highway, special issue on permafrost investigation along the Qinghai-Xizang Highway, Lanzhou Institute of Glaciology and Geocryology, Chinese Academy of Sciences*. Beijing: Science Press, 1–10, (in Chinese).

Zhou, Y., and Du, R., 1963: Preliminary investigation of permafrost on the Qinghai-Xizang (Tibetan) Plateau. *Science in China* , 2: 23–34, (in Chinese).

Zhou, Y., Guo, D., Qiu, G., Cheng, G., and Li, S., 2000: *Geocryology in China*. Beijing: Science Press, 450, (in Chinese).

Ms submitted February 2005
Ms accepted November 2006